Journal of
Marine Science and Engineering

IMPACT FACTOR 2.9

CITESCORE 3.7

Article

A Data-Driven Approach to Ship Energy Management: Incorporating Automated Tracking System Data and Weather Information

Cem Ünlübayir, Ulrich Hermann Mierendorff, Martin Florian Börner, Katharina Lilith Quade, Alexander Blömeke, Florian Ringbeck and Dirk Uwe Sauer

Special Issue
New Advances on Energy and Propulsion Systems for Ship

Edited by
Dr. Jean-Frederic Charpentier and Dr. Burak Zincir

MDPI

https://doi.org/10.3390/jmse11122259

Journal of *Marine Science and Engineering*

MDPI

Article

A Data-Driven Approach to Ship Energy Management: Incorporating Automated Tracking System Data and Weather Information

Cem Ünlübayir [1,2,3,*], Ulrich Hermann Mierendorff [1], Martin Florian Börner [1,2,3], Katharina Lilith Quade [1,2,3], Alexander Blömeke [1,2,3], Florian Ringbeck [1,2,3] and Dirk Uwe Sauer [1,2,3,4,5]

[1] Chair for Electrochemical Energy Conversion and Storage Systems, Institute for Power Electronics and Electrical Drives (ISEA), RWTH Aachen University, 52074 Aachen, Germany; martin.boerner@isea.rwth-aachen.de (M.F.B.); alexander.bloemeke@isea.rwth-aachen.de (A.B.); florian.ringbeck@isea.rwth-aachen.de (F.R.); dirkuwe.sauer@isea.rwth-aachen.de (D.U.S.)
[2] Juelich Aachen Research Alliance, JARA-Energy, 52425 Aachen, Germany
[3] Center for Ageing, Reliability and Lifetime Prediction of Electrochemical and Power Electronic Systems (CARL), RWTH Aachen University, 52074 Aachen, Germany
[4] Institute for Power Generation and Storage Systems (PGS), E.ON ERC, RWTH Aachen University, 52074 Aachen, Germany
[5] Helmholtz Institute Münster (HI MS), IEK-12, Forschungszentrum Jülich, 52428 Jülich, Germany
* Correspondence: cem.uenluebayir@isea.rwth-aachen.de; Tel.: +49-241-80-49403

Abstract: This research paper presents a data-based energy management method for a vessel that predicts the upcoming load demands based on data from weather information and its automated tracking system. The vessel is powered by a hybrid propulsion system consisting of a high-temperature fuel cell system to cover the base load and a battery system to compensate for the fuel cell's limited dynamic response capability to load fluctuations. The developed energy management method predicts the load demand of the next time steps by analyzing physical relationships utilizing operational and positional data of a real vessel. This allows a steadier operation of the fuel cell and reduces stress factors leading to accelerated aging and increasing the resource efficiency of the propulsion system. Since large ships record tracking data of their cruise and no a priori training is required to adjust the energy management, the proposed method can be implemented with small additional computational effort. The functionality of the energy management method was verified using data from a real ship and records of the water currents in the North Sea. The accuracy of the load prediction is 2.7% and the attenuation of the fuel cell's power output could be increased by approximately 32%.

Keywords: energy management; load prediction; hybrid marine propulsion system; SOFC-powered ships

Citation: Ünlübayir, C.; Mierendorff, U.H.; Börner, M.F.; Quade, K.L.; Blömeke, A.; Ringbeck, F.; Sauer, D.U. A Data-Driven Approach to Ship Energy Management: Incorporating Automated Tracking System Data and Weather Information. *J. Mar. Sci. Eng.* **2023**, *11*, 2259. https://doi.org/10.3390/jmse11122259

Academic Editors: Jean-Frederic Charpentier and Burak Zincir

Received: 1 November 2023
Revised: 26 November 2023
Accepted: 28 November 2023
Published: 29 November 2023

1. Introduction

The availability of cheap fuel and loose environmental regulations have led to shipping being an important backbone of global logistics and caused large growth in the recreational shipping sector [1]. About 3% of the global anthropogenic carbon dioxide emissions come from the shipping sector [2]. To comply with future regulations and to reduce emissions from ships, the maritime sector is looking for alternatives to internal combustion engine (ICE) propulsion systems, which currently power the majority of vessels [3]. While less-emitting propulsion systems can be retrofitted and partially replace ICEs, ships can also be redesigned implementing fully electrified powertrains. Research into zero-emission drive systems for marine applications is focused, in particular, on fuel cells and lithium-ion batteries (LIB) [4]. Ferries and other smaller vessels can already be powered entirely by batteries, as the energy density of LIBs is sufficient for these routes [5]. However, the pure battery-powered propulsion of large ships, such as container ships or cruise ships, has so far

only been the subject of concept studies and is only economically and technically feasible if the energy densities of LIBs continue to increase beyond 1000 Wh/L in the future [6]. Reducing emissions of cruise ships is important as they frequently stop at busy ports where the emission of pollutants is an additional concern in these often densely populated areas. However, large vessels cannot solely be powered by state-of-the-art LIBs because of the low energy density in comparison to the energy content of large fuel storage tanks filled with conventional fuels such as heavy fuel oil or hydrogen. Hence, hybrid drivetrains are of interest to fulfill the power and energy requirements.

A solid oxide fuel cell (SOFC) is a viable and potentially sustainable alternative to replace conventional means of propulsion because it operates at high temperatures, enabling the utilization of process and excess heat and achieves high electrical efficiencies [7]. In [8], a lab-scale SOFC was operated for more than 100,000 h which proves the longevity of the component under laboratory conditions. SOFCs are particularly relevant for the maritime sector due to their compact design, high power density, and compatibility with various fuels like hydrogen, ammonia [9], or methane [10]. SOFCs operate at elevated temperatures between 600 and 1000 °C [11]. A portion of the process heat and the heat generated from energy conversion within the cells can be utilized in the ship's heating system, further increasing system efficiency. These features make SOFCs suitable for providing electrical and thermal power for vessels, enabling greater energy efficiency and reduced greenhouse gas emissions compared to conventional ICE-powered propulsion systems. SOFCs have a comparably slow responsiveness towards electrical load changes, which was investigated by Obara et al. in [12]. Therefore SOFCs are typically supported by secondary power sources such as LIBs or supercapacitors to compensate for the low dynamic capabilities of the SOFC depending on the application [13]. Zhang et al. [14] have studied the utilization of SOFCs coupled with supercapacitors in microgrids and considered the slow dynamic responsiveness in their energy management development without utilizing additional data sources to forecast load events or applying machine learning to reduce stress factors on the SOFC. However, their work has not followed a generic approach for the implementation of the EMS and therefore cannot be easily adapted to other applications. Wu et al. [15] studied an SOFC–engine hybrid power system, which could be used in marine applications due to the fuel flexibility of SOFCs. Their approach does not eliminate local emissions and the dynamic load components that cannot be provided by the SOFC might not be compensated by the motor.

While SOFCs appear to be a promising alternative to engine-powered powertrains, there are still challenges and considerations that need to be addressed before widespread market introduction is possible. Until now, there have only been a few drive concepts for vessels in which SOFCs have been used or investigated. A 150 kW SOFC using natural gas as fuel has been implemented in a cruise ship [16]. However, a fuel cell of this size is at best suitable as a retrofit solution to replace ICEs. Within the German research project SchIBZ, a 50 kW diesel-powered SOFC for a marine application was investigated [17]. Diesel-powered SOFC systems have a higher efficiency than conventional diesel engines but still produce exhaust gases and nitrogen oxides in the diesel fuel processing or reforming process. As part of the European NAUTILUS project, a 60 kW SOFC for different fuel types is being developed for a cruise ship [18]. Consequently, fuels that do not emit any greenhouse gases are being investigated as part of this research work, which in the long term will enable the targeted emission-free shipping. However, SOFC technology has not yet been scaled up. This is also reflected in the costs incurred for the installation of an SOFC. While conventional powertrains cost between 250 and 300 EUR /kW, SOFCs require an investment of 2000 EUR /kW [19]. Van Biert et al. [20] also describe the low level of technological maturity and the mechanical vulnerability as additional factors that hinder the widespread adoption of this technology in the maritime sector. It is therefore essential to examine the service life of SOFCs more closely and to reduce stress factors that lead to premature degradation.

Investigating the aging mechanisms of SOFCs is an important aspect of research to prepare the technology for commercial use in various applications. In long-term operation under static laboratory conditions, a lifetime of a short SOFC stack of up to 11.5 years of operation was achieved [8]. As large ships have service lives of several decades [21], a long service life is economically attractive for this type of application. If SOFCs are operated with dynamic power outputs, they undergo thermal cycling as the temperature in the stacks changes with power fluctuations which can increase the area surface resistance of the fuel cell [22]. This thermal cycling can cause mechanical degradation within the cell, such as delamination and crack formation at the interfaces between the respective electrode and the electrolyte [23]. Thus, it can be assumed that the steady-state operation of a SOFC is beneficial for its longevity. Hence, SOFCs are not suitable for load-dynamic applications and must be supplemented by another component such as a battery or supercapacitor as cycling stresses the materials of SOFC and leads to accelerated degradation.

The development of efficient EMSs for the power distribution between the propulsion components of hybrid propulsion systems is an essential element in the electrification of marine propulsion systems. For the EMS to achieve optimal overall efficiency of the powertrain, it is necessary to operate the individual power system components in efficient operating ranges. This can be achieved by operating the fuel cell in its most efficient operating range. Ma et al. [24] have investigated a rule-based energy management method for a fuel cell–battery hybrid vessel, aiming to reduce stress factors on the battery to extend the longevity of the component. The size of each drive component should be in proportion to the savings that can be achieved by extending its service life. Dinh et al. [25] studied an EMS based on equivalent fuel consumption minimization for a hybrid vessel drivetrain powered by an ICE and a battery, which aims to maximize the efficiency of the engine generators. However, only load sections in which dynamic positioning is carried out were examined. Bui et al. [26] have developed a real-time capable EMS for a diesel generator and battery-powered hybrid propulsion system, enabling efficient dynamic positioning of ships and validating the control logic in a hardware-in-the-loop environment. Bassam et al. [27] have studied various energy management methods for a hybrid fuel cell–hybrid ferry application focusing on the minimization of fuel consumption using characteristics of a real ship. However, no stress factors were investigated that could lead to accelerated degradation of the components, which could increase operating costs in addition to fuel costs. Kistner et al. [28] have also considered the slow dynamic responsiveness of the SOFC in their optimization approach for the dimensioning of hybrid ship concepts. Characteristics and the dynamic behavior of the SOFC were considered, but no further data from ship operation were considered. In recent years, machine learning-based algorithms have become increasingly popular in energy management research [29]. The rapid increase in computing power enables the development of complex methods for predicting load events. This enables the control of an energy management system (EMS) for a marine application using model predictive control [30]. However, the resource-intensive training phases of machine learning algorithms or the high requirements on the computing power of the controller pose major obstacles to widespread use in energy management, burdening the achievement of real-time responsiveness necessary for efficient energy optimization.

Since ships are often cruising in densely trafficked waters, the surrounding area must always be monitored to avoid collisions. In addition to radar systems that enable a direct analysis of the surroundings, the automatic identification system (AIS) is an important instrument in modern shipping. Through AIS, ships continuously transmit information about their position, speed, direction, and destination via radio [31]. These signals can be received by base stations and other vessels. AIS has been continuously enhanced and is also subject to research in the field of data mining for maritime research [32]. Kim et al. [33] have utilized AIS data to estimate the operational efficiency of ships to calculate fuel consumption without data from the drive train. However, no EMS has been developed that uses the AIS data to operate the vessels more efficiently.

To the best knowledge of the authors, no efforts have been made to develop an EMS for a large vessel that takes tracking and weather information into account to predict upcoming load events. Through the integration of the following main contributions, this work seeks to close the previously described research gap:

- Development of an energy management method for ship propulsion systems powered by SOFCs and batteries utilizing authentic cruise ship power profiles, tracking data, and weather information.
- The implementation and enhancement of data-based load prediction algorithms within the energy management to increase the efficiency of the propulsion system.
- Improvement of the load distribution to better conform with the dynamic behavior of the SOFC to extend its lifetime and increase the resource efficiency of the propulsion system.

Furthermore, this work extends the existing research with the following secondary contributions:

- Introduction of a method using physical relationships between the characteristics of the ship and its flow properties.
- Verification of the functionality of the proposed data-based energy management method based on real data from cruises.

2. Drive Train and Data Sources for Modeling

In the following sections, the basic principles of the hybrid drive train as well as the data basis for the development of energy management algorithms are described.

2.1. Hybrid Propulsion System

For the electrification of a cruise ship, a modular and scalable propulsion system, whose topology is shown in Figure 1, is suggested. The drive train of the vessel is powered by an SOFC system to cover the base load and a LIB to provide the dynamic load components. The following cruise ship propulsion system will be simulated:

- $P_{SOFC,min}$ = 0 W
- $P_{SOFC,max}$ = 45 MW
- E_{Bat} = 5 MWh
- $P_{Bat,max}$ = 10 MW (or 2C)

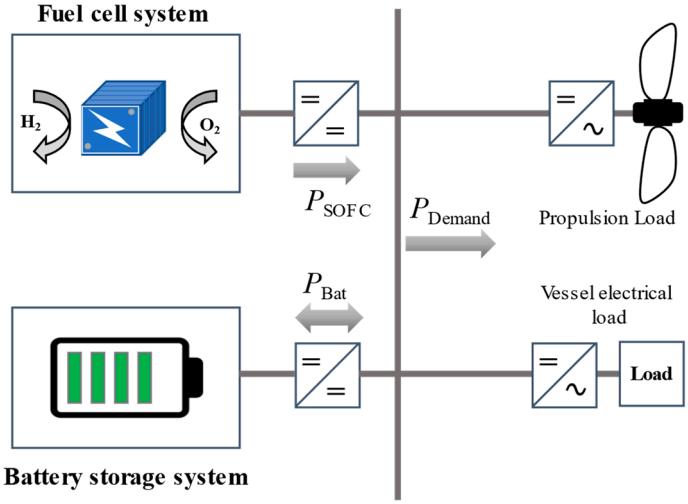

Figure 1. Topology of a fuel cell–battery hybrid propulsion system.

The overall electrical power P_{Demand} consists of the power demand required for propulsion ($P_{Propulsion}$) and the electrical load or hotel load (P_{Hotel}); P_{SOFC} represents the fuel cell's output power, and P_{Bat} represents the battery system's in- or output power,

depending on whether the battery is being charged or discharged. The temporal resolution of the calculation was set to $\Delta t = 15$ min matching the resolution of the power demand data set. Such a resolution is plausible to accurately develop an EMS for a cruise ship application due to the high inertia of large ships in comparison to other electric vehicle applications such as cars. In the simulation, no distinction is made between the propulsion load and the hotel load, as these loads cannot be decoupled in the electrical intermediate circuit of the ship topology under investigation.

A section of the load profile, which was used as a basis for the development of energy management, can be seen in Figure 2. The data set comprises a measured load profile of a large cruise ship from 2019. The sample rate is 15 min. At the harbor, the investigated cruise ship has a total electrical power demand below 10 MW (where P_{Hotel} is dominant). At sea or during maneuvering, the total electrical power demand is above 10 MW. The harbor mode can be repeatedly observed in Figure 2, e.g., between t = (2, 3). At sea, the total electrical load demand mainly depends on speed and weather conditions. Specifications of the cruise ship are shown in Table 1.

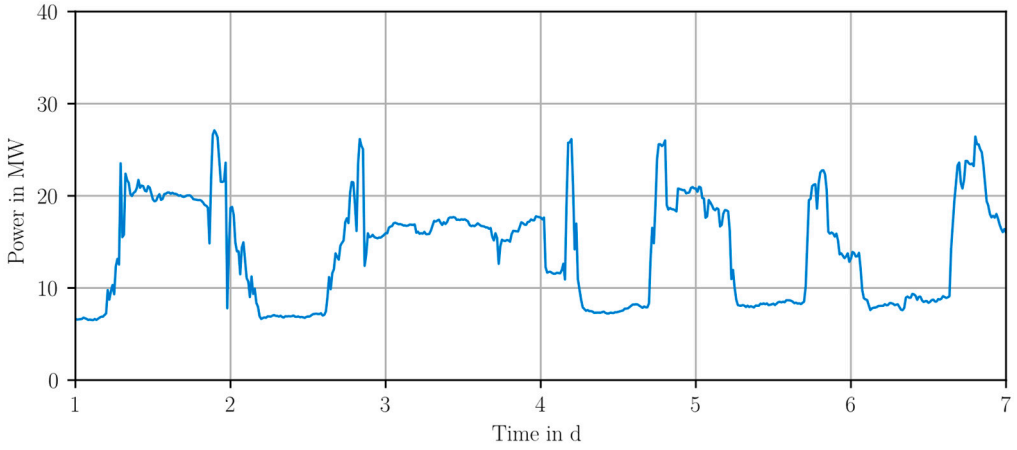

Figure 2. Measured load profile of the vessel propulsion load and hotel load for seven days during summer.

Table 1. Specifications of the investigated vessel.

Specification	Value	Details
Ship size	127,000 GRT	1 gross register tonnage (GRT) = 100 cubic feet ≈ 2.83 m^3
Ship length	300 m	
Maximum electrical power demand	46.8 MW	Sum of propulsion power demand and hotel power demand
Draft (hull)	8.1 m	
Maximum speed	22 knots	22 knots = 40.74 km/h

2.2. Hydrodynamic Aspects

For speeds below hull speed, the power requirement P_{Demand}, which a ship must continuously apply to maintain a certain velocity v_w through the water, can be approximated by a cubic relationship [34]:

$$P_{\text{Demand}} \propto v_w^3 \tag{1}$$

On calm waters, the proportionality factor depends solely on the design and surface properties of the hull. In waters where ships navigate, there are usually currents of various types. Larger global ocean currents overlap with tides, currents at river mouths, wind-induced movements, or other local effects to form a diverse current pattern, which can vary in strength depending on the water depth [35].

On the left side of Figure 3, a schematic drawing of a ship traveling through the water at a certain speed over ground v_g is shown. This speed can be determined, for example, using a satellite navigation system such as a Global Positioning System (GPS). At the same time, the ship is exposed to the velocity of ocean currents, which is indicated by v_c in Figure 3. The water resistance in such a case does not result directly from the speed over ground v_g, but from the actual speed of the ship through water, which is influenced by the currents. In the right part of Figure 3, it is shown how to calculate the velocity through the water v_w as the difference between the velocity vectors v_g and v_c.

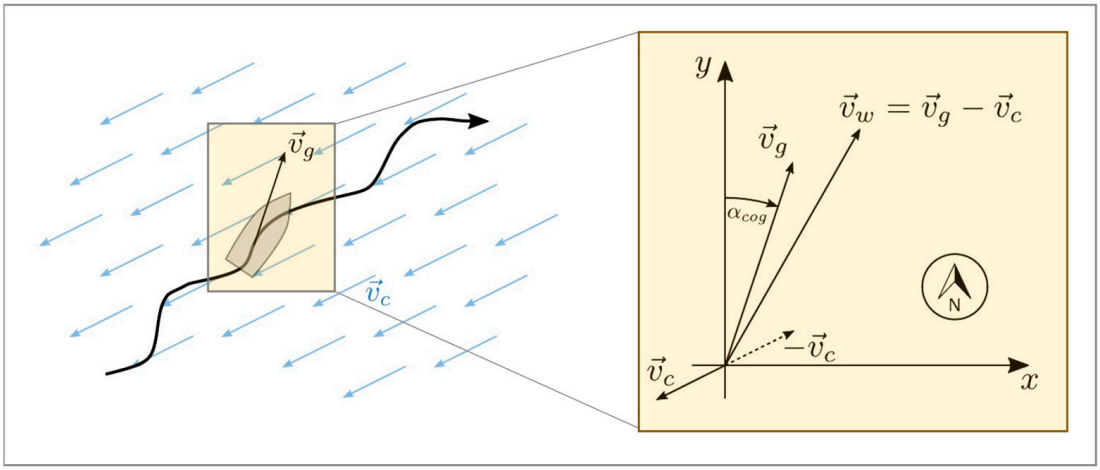

Figure 3. The influence of currents on a ship with some trajectory shown as a black wavy arrow and the relationship between the different speeds v_w, v_g, and v_c in a coordinate system.

2.3. Losses in the Drive Train

In addition to all flow resistances to which the ship is subjected when moving through the water, there are also other inefficiencies in the drivetrain that increase the power requirement. High power losses, especially in the transmission of the power of the turning machine to the movement of the ship through the water with the help of a ship's propeller are present. Ship propellers typically have efficiencies in the range of 50 to 70% [36], depending on the design and speed of travel. The propeller efficiency is defined as the ratio of the thrust power and the shaft power. Furthermore, the losses of power electronic components such as converters and inverters also decrease the overall efficiency of the drive train. Power electronics built into drivetrains with power ratings of several MW typically have efficiencies of well above 80% under normal load conditions [37]. In this work, the losses of power electronics have implicitly been considered in the calculation but have not been modeled or mapped within the simulation framework.

2.4. Data Collection

As described above, many vessels continuously transmit position, speed, and other cruise data via the AIS system. This data is not only continuously provided to other ships but also collected and archived by government agencies and numerous commercial organizations. Since the investigated cruise ship was underway in areas of the North Sea, where a good data basis was present, the development and verification were restricted to this region. The archives listed in Table 2 were considered. In the period from April to October 2019, the vessel was cruising in European waterways. The route of the vessel during parts of this period known from the AIS data is shown in Figure 4. In Figure 4, areas for which flow data from the Federal Maritime and Hydro-graphic Agency of Germany (German: Bundesamt für Seeschifffahrt und Hydrographie, short BSH) were received are shown in addition to AIS data.

Table 2. Overview of investigated data archives for ship tracking and coastal area characteristics.

Source	Data Type	Details
Federal Maritime and Hydrographic Agency of Germany (German: Bundesamt für Seeschifffahrt und Hydrographie, short BSH)	Current data and AIS	Current data for the North Sea and in somewhat higher spatial resolution for the German Bight from observations and estimates based on physical models
Danish Maritime Authority	AIS	Data from all ships that have sailed in waters surrounding Denmark
Norwegian Coastal Administration	AIS	Data from ships worldwide with varying resolution
United Nations	AIS	Data from ships worldwide with varying resolution

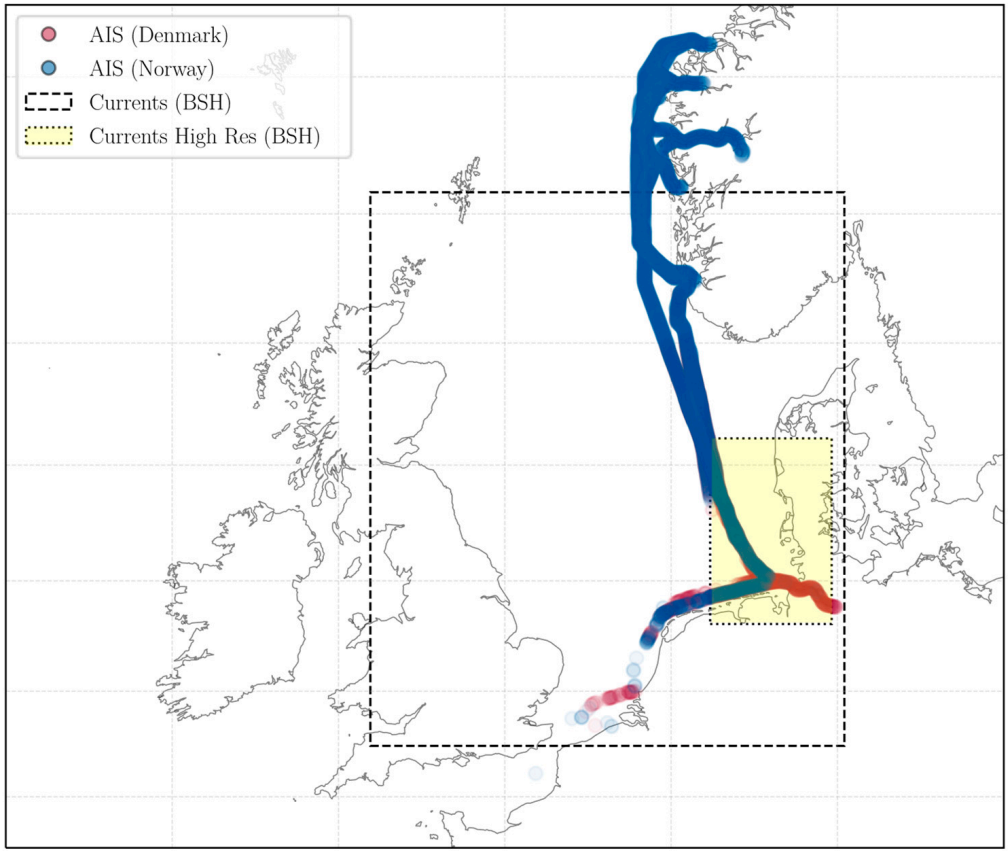

Figure 4. Route of the vessel in Europe from AIS- data in summer 2019 shown in the larger dotted rectangle and areas with higher resolution current data shown in the yellow highlighted smaller dotted rectangle.

Because of the good data basis of the North Sea waters, the development and verification of the energy management methods were restricted to these data sets.

2.5. Processing of the Collected Data

The utilized data sets have gaps, in which the recording was interrupted. Both the load consumption data and the AIS data have gaps of varying lengths. For analyses such as the simulation of an EMS method or the evaluation of the quality of a prediction of the ship's load demand, it is helpful to not only consider individual 15 min segments (i.e., individual data points) but also analyze longer periods with consecutive data points. These periods will be called episodes in the following and are described in Table 3. Since certain dynamic effects, such as the trajectory of the battery's state of charge (*SOC*), must be analyzed for the evaluation of an EMS, only episodes of at least 12 h in duration are considered. Based on

similarities in the routes traveled during the identified episodes, the episodes are assigned to groups I to III. Figure 5 shows the corresponding route of the episodes on a map of the North Sea for the three groups.

Table 3. Selected episodes in the selected region with consecutive data points from 2019.

Name	Group	Start Time (UTC)		End Time (UTC)		Duration in hh:mm
A	I	May 19	08:30	May 20	02:45	18:15
B	I	Jun 09	11:15	Jun 10	02:15	15:00
C	II	Jun 13	20:30	Jun 14	16:00	19:30
D	III	Jun 28	13:30	Jun 29	04:15	14:45
E	I	Jun 30	01:45	Jul 01	02:15	24:30
F	II	Jul 04	20:30	Jul 05	13:15	16:45
G	I	Jul 21	07:15	Jul 22	02:30	19:15
H	II	Jul 25	20:30	Jul 26	13:00	16:30
I	I	Aug 11	11:30	Aug 12	02:45	15:15
J	I	Sep 21	22:45	Sep 23	01:30	26:45
K	II	Sep 26	16:00	Sep 27	04:45	12:45

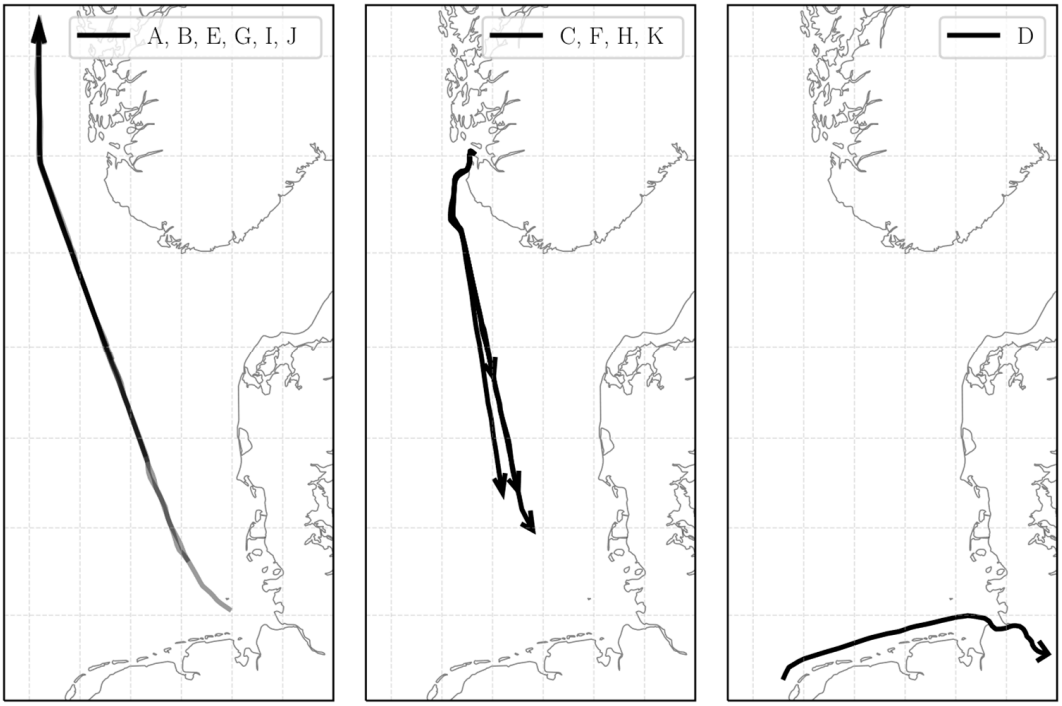

Figure 5. Visualization of the selected episodes of the investigated cruise ship on the North Sea coast of Germany, the Netherlands, Denmark, and Norway, of Group I (**left**), Group II (**center**), and Group III (**right**); the routes are indicated by black arrows.

Some routes with a southward trajectory that end or begin in the middle of the North Sea can be noticed. At these points, the ship continued traveling until reaching a harbor, but gaps were present in the AIS data before the beginning or after the end of the respective episodes. The abrupt end of the routes in group I in the northern area is due to the geographical limitations of BSH data.

Figure 6 shows the measured load profiles of the episodes. Since there are longer breaks between the episodes due to incomplete data, as shown in Table 2, the load profile is not shown as a continuous line but with breaks in between.

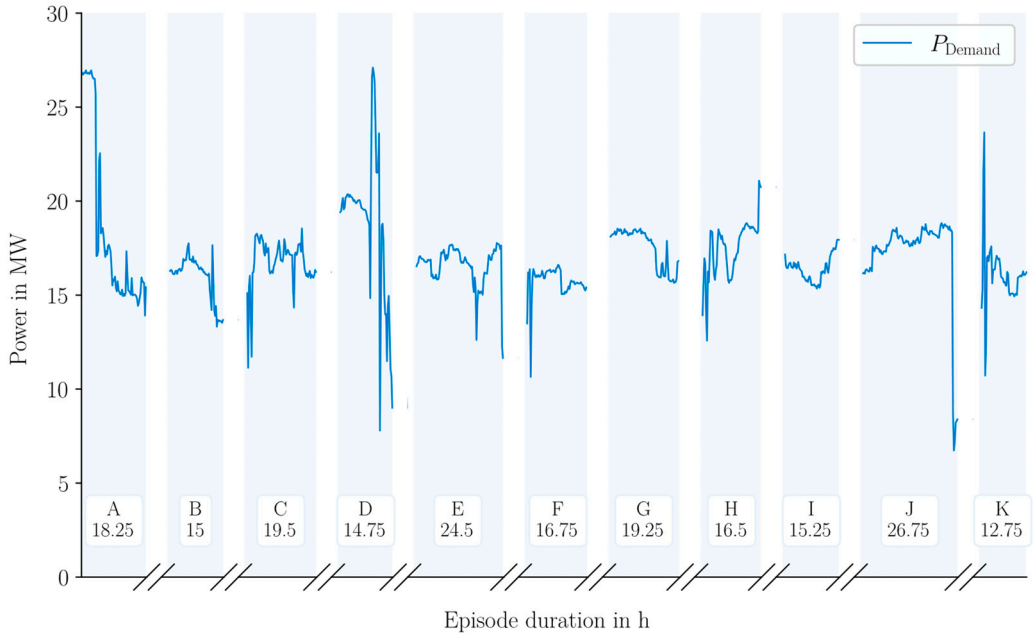

Figure 6. Measured 15 min load demand of episode A–K. The individual episodes are highlighted in light blue and separated by break intervals which are scaled equally.

3. Simulation of Propulsion Components and Energy Management Development

In this chapter, the simulation of the battery and fuel cell as well as the development of the control methods for the efficient distribution of power between the components is described. Based on the previously discussed fundamentals and data, a rule-based energy management method will be considered as a reference for the improved EMS. The functionality of this improved method will be verified with simulations. For the development of an EMS, a simulation of the system components is necessary to evaluate and verify strategies without applying them directly in real applications. Python was used in this work as the programming language to create the simulative framework.

3.1. Modeling of the Battery

To model the electric performance of the LIB as well as the thermal losses, the equivalent circuit model (ECM) shown in Figure 7 was used. The ECM consists of a voltage source, resistors representing ohmic and polarization resistances, and capacitors representing polarization capacitances within the battery cell [38]. Measurements on a battery cell were carried out and used to fit the ECM. The electrical and thermal behavior is simulated with the ISEAFrame [39], which is an open-source program for battery simulation.

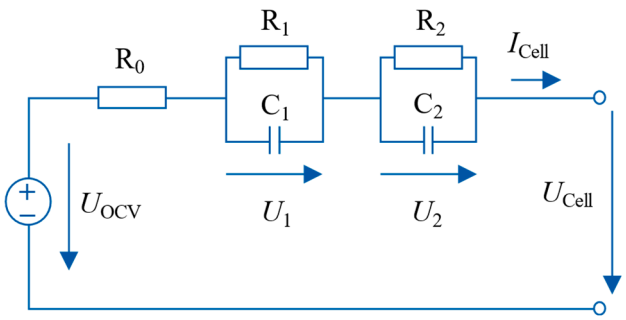

Figure 7. Equivalent circuit model of a battery cell.

The open circuit voltage U_{OCV} of the battery, which can be measured without an applied load at the terminals of the battery, is the result of the internal structure of the battery and mainly depends on the state of charge, which is given as a percentage value

between 0 and 100% and can be compared to a fuel level indicator of a vehicle. U_{OCV} can be measured when no load is connected to the battery and all diffusion processes have completely decayed. As soon as the battery is charged or discharged, the output voltage of the battery rises or drops due to the voltage drop across the elements of the ECM [40]. In the unloaded state, U_{OCV} and U_{Cell} are equal. The electrical parameters of the battery can be found in Table 4. The voltage across the parallel connection of resistance and capacitance is calculated as follows:

$$\dot{U}_i = -\frac{1}{R_i \cdot C_i} \cdot U_i + \frac{1}{C_i} \cdot I_{Cell}. \quad (2)$$

Table 4. Electrical parameters of the battery cell.

Description	Value
C_{Cell}	64 Ah
Nominal cell voltage	3.7 V
Cell voltage range	3.0–4.2 V
R_0	$0.75 \times 10^{-3} \ldots 1.70 \times 10^{-3}$ Ω
$\tau_1 = R_1 \cdot C_1$	13.04 . . . 100.00 s
$\tau_2 = R_2 \cdot C_2$	385.54 . . . 1.00×10^4 s

The *SOC* is calculated by

$$SOC = SOC(t_0) + \frac{\eta}{C_{Cell}} \int_{t_0}^{t_0+t} I_{Cell} dt, \quad (3)$$

where η is the coulomb efficiency and C_{Cell} is the nominal capacity of a single battery cell. To simulate the input current of a single cell, the input power is scaled down on the battery model's input side. To simulate the voltage of the entire battery system, the output side battery voltage is scaled up.

3.2. Modeling of the Fuel Cell

Given that the EMS strategies are deployed on certain test sets, a simple modeling of the SOFC is sufficient, which does not consider reactions such as heat conversion. Figure 8 shows a qualitative illustration of the fuel cell's output power P_{SOFC} which follows the power demand signal $P_{SOFC,demand}$ considering the safe boundaries of operations within the interval ($P_{SOFC,min}$,$P_{SOFC,max}$) and the limit of the rate of change of the output power. The maximum dynamic rate to operate the fuel cell $\Delta P_{SOFC,max}$ is set to $2\frac{\%}{min} \cdot P_{SOFC,max}$.

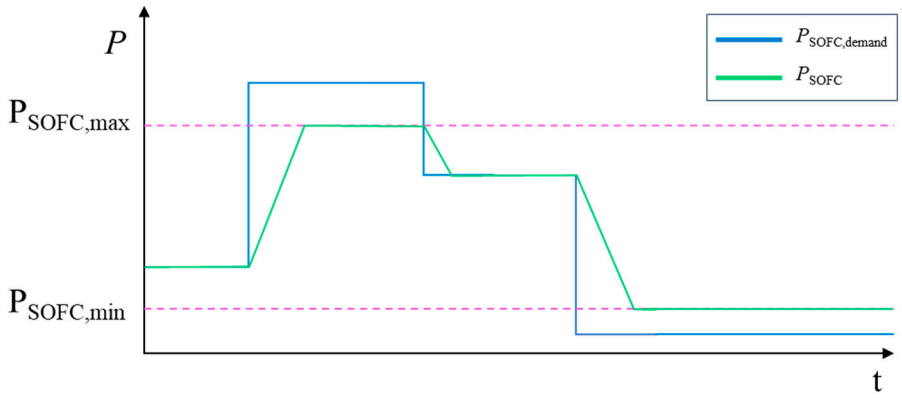

Figure 8. Modeling of the output power of a SOFC P_{SOFC} concerning the input power $P_{SOFC,demand}$.

Evaluation Criterion for the Attenuation of the Power Output Behavior of the SOFC

To assess the influence of dynamic load processes in the context of the developed energy management methods, a criterion is introduced that cumulates the rate of change of the fuel cell for each investigated episode. For each time range between two data points

from the load profile with n samples, the RMS of the rate of change $\frac{dP_{SOFC}}{dt}\left[\frac{W}{s}\right]$ will be cumulated for an entire episode, yielding a score for the dynamic behavior of the SOFC:

$$Score_{Attenuation} := \sqrt{\frac{1}{t_n - t_0}\sum_{i=1}^{n}\frac{(P_i - P_{i-1})^2}{t_i - t_{i-1}}}, \tag{4}$$

where a higher score could lead to the accelerated aging of the SOFC due to thermal cycles which is a dominant stress factor for SOFCs causing irreversible damage to the active materials.

3.3. Rule-Based Energy Management Method

The SOFC is used to provide the base load of the ship's electrical power demand and the battery serves as a buffer to compensate for load transients and peak loads. It is therefore possible to define a simple energy management method with only a few rules:

$$P_{\text{SOFC,demand}}(t) = P_{\text{demand}} + c(t)\cdot P_{\text{charge}}, \tag{5}$$

$$P_{\text{Bat}}(t) = P_{\text{demand}}(t) - P_{\text{SOFC}}(t), \tag{6}$$

here $c(t)$ represents the time-dependent charge or discharge factor of the battery with hysteresis. P_{charge} is hereby a constant charge or discharge power, which varies according to the *SOC*. The essential idea of this strategy is that the energy management method attempts to meet the total load demand with the SOFC, and that the battery is used to balance the differential load in case the SOFC cannot respond sufficiently to dynamic load events. Since, with such a strategy, the battery could either continue to become increasingly discharged or fully charged over time, depending on the load demand, there is still compensation if the *SOC* falls outside the safe operating windows. Therefore, the safe operating depth of discharge can be kept low to avoid a sudden reach of the end of charge or discharge voltage, e.g., within 30% to 70% *SOC*. Figure 9 shows a simulation of this strategy using the load profiles and the models described in the fundamentals.

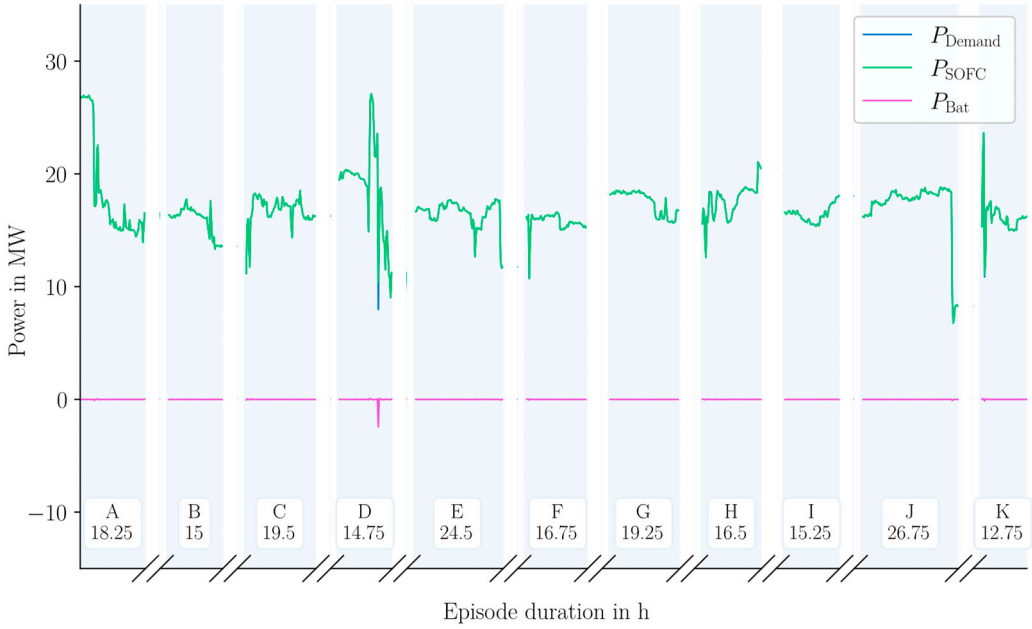

Figure 9. Power distribution in the simulation of the rule-based energy management method of the different episodes.

The simulation shows that this basic rule-based energy management method manages to fulfill the fundamental task formulated in Equations (5) and (6) but also shows its

disadvantages. Figure 9 shows that the battery is not used intensively, and the SOFC is operated in a wide power range.

3.4. Development of a Load Demand Estimator

In the following, a prediction for the load demand to distribute the load between the propulsion components more efficiently by using the battery more intensively and decreasing the dynamic operation of the SOFC is developed.

Using the processed data, the estimation functions for the different load components of a cruise ship are empirically derived and integrated to provide an estimator for the entire load demand. For the development of the estimator, the measured baseload at port will be analyzed first, before the power demand of the subsequent time steps is estimated by looking at the relationship between speed and power demand while at sea.

3.4.1. Empirical Analysis of the Base Load

The base load of the vessel results from the thermal and electrical requirements of the hotel operation as well as other various consumers, such as signaling systems or a minimum load that the machines shall always provide. To determine this base load from the data, periods in which the ship is in port are considered. In the 15 min load profiles of the cruise ship, there are markers indicating whether the ship was located in a harbor or not. In Figure 10, all recorded load demand measurements at which the ship was docked in a harbor are shown. To utilize the data for the development of the EMS, a look-up table consisting of the arithmetic mean for each time step of a representative day has been created. The resulting look-up table values and the considered data are shown in Figure 10. The more data points exist for one given time, the more data points in a harbor have been recorded.

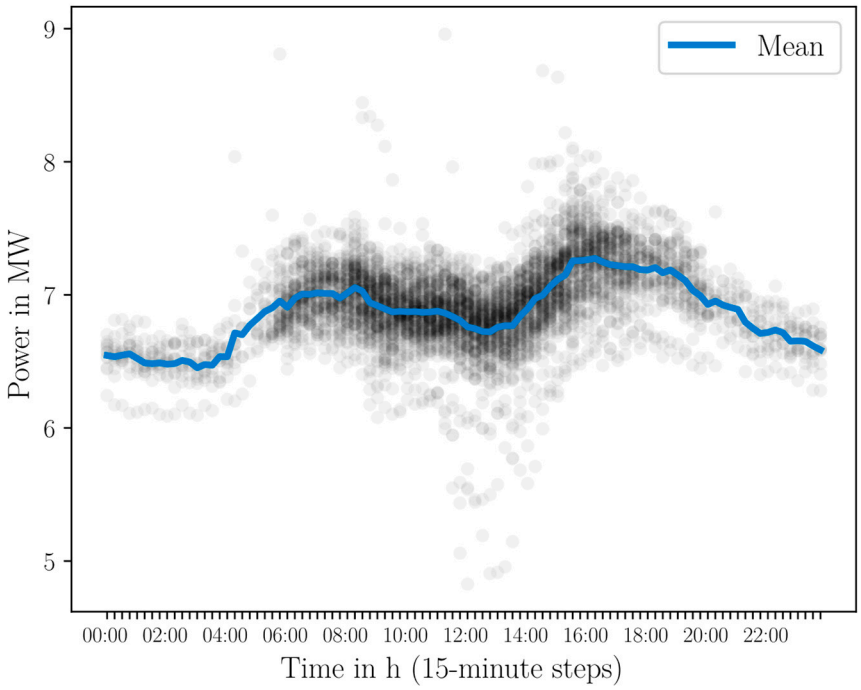

Figure 10. Arithmetic mean of load demand shown as a blue line and collected data points in harbor mode as black points for every time of the day.

It can be seen that this mean value fluctuates over the course of the day, i.e., between t = 6:00 and 18:00. and that the fluctuations are smallest at night. The mean value is considered as the base load and stored as $\hat{P}_{\text{Baseload,15min}}(t)$ for further analysis.

3.4.2. Analysis of the Propulsion Load

In Figure 11 the measured load of episode D with a total duration of 14:45 h is shown. Additionally, mean velocity magnitudes over ground v_g and velocity magnitudes through the water v_w are shown in the graphs. A relationship between the speed of the ship and its power requirements can be seen. It is also evident that the power requirement increases during acceleration. At the same time, it can be observed that, after the first drop at t = 32, v_g increases again to approximately the value the ship had at the beginning of the episode. However, the power demand rises to a higher value and stays there for a while. A somewhat stronger increase can initially be explained by an acceleration of the ship and the power to be applied for this purpose to increase the kinetic energy. However, since the power requirement remains at a higher value beyond this, this is not sufficient as an explanation. At this point, other effects occur that increase the power requirement of the ship. These are ocean currents, for example, which influence the speed through the water and thus the power demand at the same speed over ground. It can be observed that the speed over ground corrected with the current data, i.e., the speed through the water v_w follows the course of the power more closely.

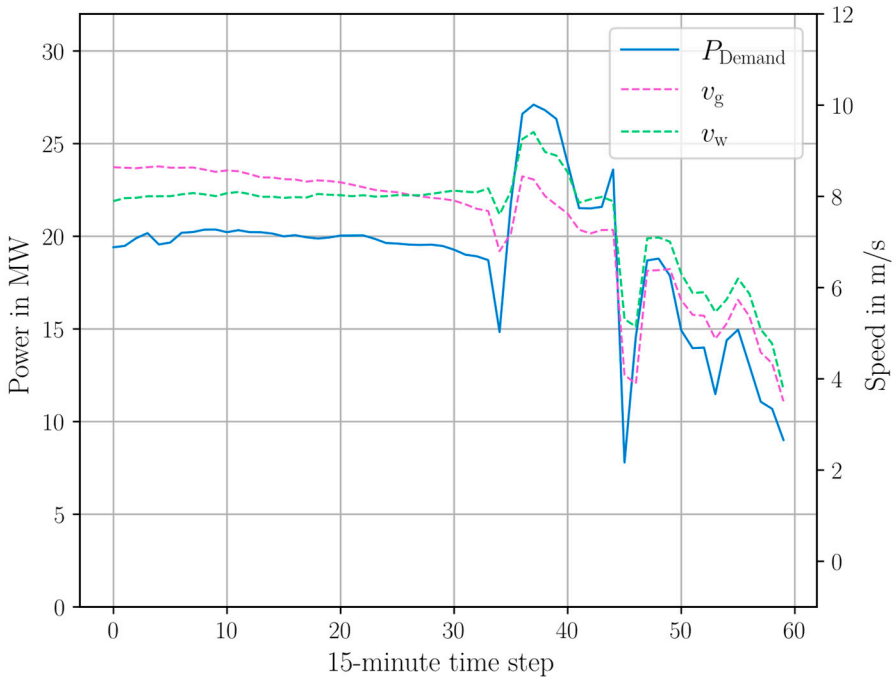

Figure 11. Power demand and velocities v_w and v_g.

Since suitable data to describe the velocities and flows quantitatively are available, a physical relationship to the power demand can be drawn. To maintain a constant speed through the water v_w, a power P_v must be applied due to the water resistance:

$$P_v(t) \approx d \cdot v_w(t)^3, \tag{7}$$

with

$$v_w(t) = \left\| \vec{v}_w(t) \right\| \begin{pmatrix} \sin \alpha_{COG}(t) \\ \cos \alpha_{COG}(t) \end{pmatrix} = \left\| \vec{v}_g(t) - \vec{v}_c(t) \right\| \begin{pmatrix} \sin \alpha_{COG}(t) \\ \cos \alpha_{COG}(t) \end{pmatrix}. \tag{8}$$

The cubic coefficient d will be fitted in the further development and an angle α_{COG} which represents the direction of the vector v_w is present as shown in Figure 3. AIS data do not provide the vector of the speed but the length of the vector and an angle α. Considering

the relation between kinetic energy and propulsion power, the change in power after a time step at time t can be described as follows:

$$\Delta\hat{P}_{kin,15min}(t) = \eta_{eff} \cdot m \cdot \frac{1}{\Delta t}\left(\vec{v}_{g,15min}(t) \cdot \Delta\vec{v}_{g,15min}(t) - \frac{1}{2}\Delta\vec{v}_{g,15min}(t)^2\right). \quad (9)$$

Equations (7) and (9) form a system of equations, whose only unknown constants are η_{eff}, m, and d. With the help of the least squares method, a curve is fitted to obtain the empirical relationship between the recorded velocity of the ship $v_{w,}$ and the power demanded for propulsion, which can be seen in Figure 12. The values $d \approx 2.4420 \cdot 10^4 \frac{\mathrm{Ns}^2}{\mathrm{m}^2}$ and $\eta_{eff} \cdot m \approx 3.7735 \cdot 10^7$ kg are obtained. Assuming an efficiency of the drive train of $\eta_{eff} = 70\%$, including the transmission of power through the ship's propeller, a mass of $m \approx 53.9 \cdot 10^6$ kg is obtained, which may correspond to the estimated displacement weight of a cruise ship. The exact mass of the ship is not known, but the order of magnitude is plausible.

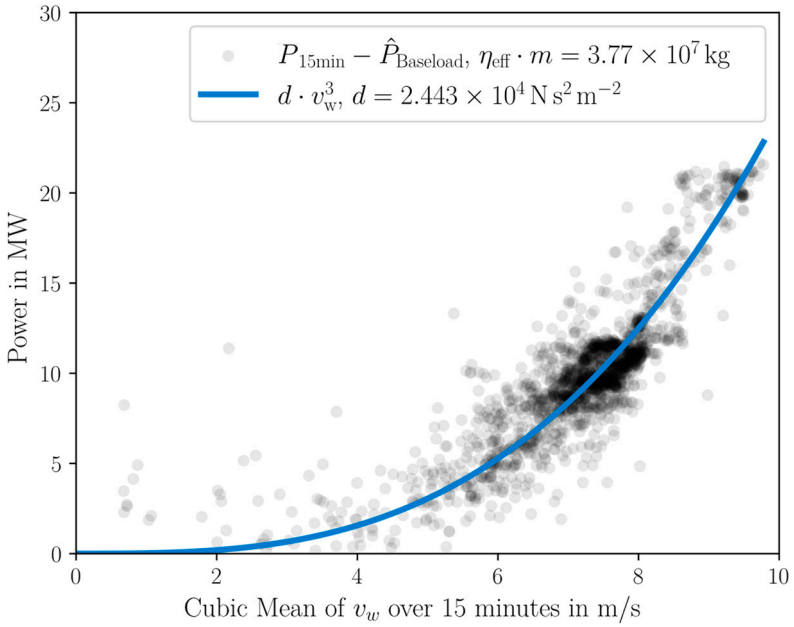

Figure 12. Relation between measured power demand values and speed of the vessel shown as a curve fit.

An estimation of the mean total power demand of the ship at a time t with known mean velocities in the interval $(t - \Delta t, t)$ as well as velocity changes compared to the last time interval is thereby possible:

$$\hat{P}(t, v_g, \Delta v_g, v_w) = \hat{P}_{\mathrm{Baseload}}(t) + P_{\mathrm{v}}(t, v_w) + \Delta\hat{P}_{kin}(t, v_g, \Delta v_g). \quad (10)$$

4. Results

In this section, the results of the data analysis and processing, as well as the performance of the energy management method, will be described in detail.

4.1. Estimation of the Total Load and Power Requirement of a Vessel

In the following, a comparison of the estimates of the total load with the measured load profiles for the eleven episodes A to K is conducted. Figure 13 shows P_{Demand} and the estimation as $P_{\mathrm{est}} = \hat{P}(t, v_g, \Delta v_g, v_w)$ as well as the deviation of P_{est} with respect to P_{Demand}. The mean deviation for all episodes is 7.68%.

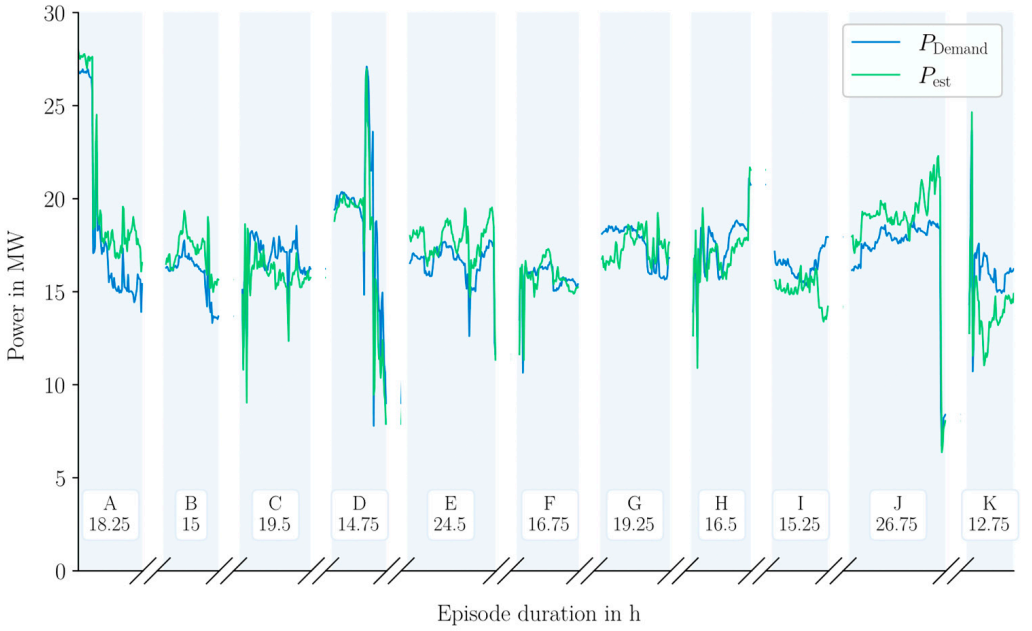

(**a**)

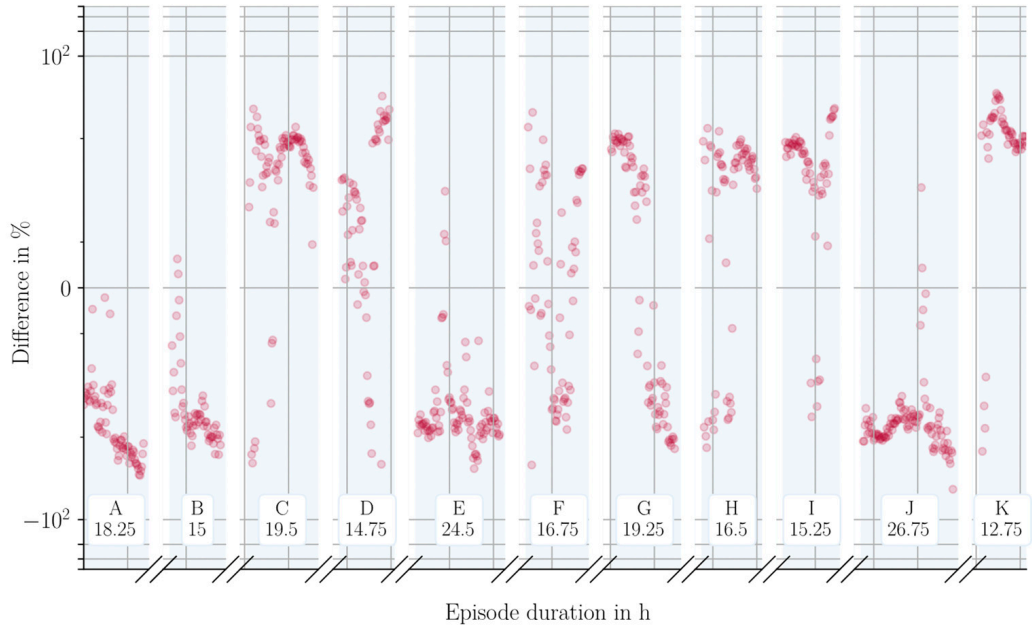

(**b**)

Figure 13. Comparison between measured and estimated load with (**a**) the load curves; (**b**) the deviation of the estimated values P_{est} from the measured values P_{Demand} in percent shown on a logarithmic scale as red points.

The errors of neighboring time steps are not independent of each other but seem to be related, i.e., overestimation or underestimation continue for consecutive data points in an episode. The deviation appears to be systematic. To improve the estimator, an iterative algorithm can be used that computes an error tracker $\text{Err}_{\text{tracker}}(t + \Delta t)$ to reduce the difference $\text{Err}_{\hat{P}}(t)$ between the estimate $\hat{P}(t)$ and the measurement. $\text{Err}_{\hat{P}}(t)$ is calculated as follows:

$$\text{Err}_{\hat{P}}(t) = P_{\text{Demand}} - \hat{P}_{est}, \tag{11}$$

The tracker $\mathrm{Err}_{\mathrm{tracker}}(t+\Delta t)$ and the filtered estimate $\hat{P}_{\mathrm{est.,filtered}}(t)$ are calculated iteratively as follows:

$$\mathrm{Err}_{\mathrm{tracker}}(t+\Delta t) := p \cdot \mathrm{Err}_{\mathrm{tracker}}(t) + q \cdot \mathrm{Err}_{\hat{P}}(t), \tag{12}$$

as well as

$$\hat{P}_{\mathrm{est.,filtered}}(t) := \max\left[\hat{P}_{est}(t) + \mathrm{Err}_{\mathrm{tracker}}(t), \hat{P}_{\mathrm{baseload}}\right], \tag{13}$$

in which the filtered power $\hat{P}_{\mathrm{est.,filtered}}(t)$ guarantees that the estimated values do not fall below the baseload of the vessel since those values will be assumed as implausible. To obtain the best load estimate, the parameters p and q were varied, while satisfying the constraint $p + q = 1$. The estimate with the lowest MAPE was achieved by the factors p = 0.3 and q = 0.7, which is shown in Figure 14. Figure 15 shows P_{Demand} and the filtered estimation as $P_{\mathrm{est.,filtered}}$ as well as the deviation of $P_{\mathrm{est.,filtered}}$ and P_{Demand}. The mean deviation for all data points is 2.67%. Compared to the unfiltered estimator, a clear improvement in the estimated values can be seen.

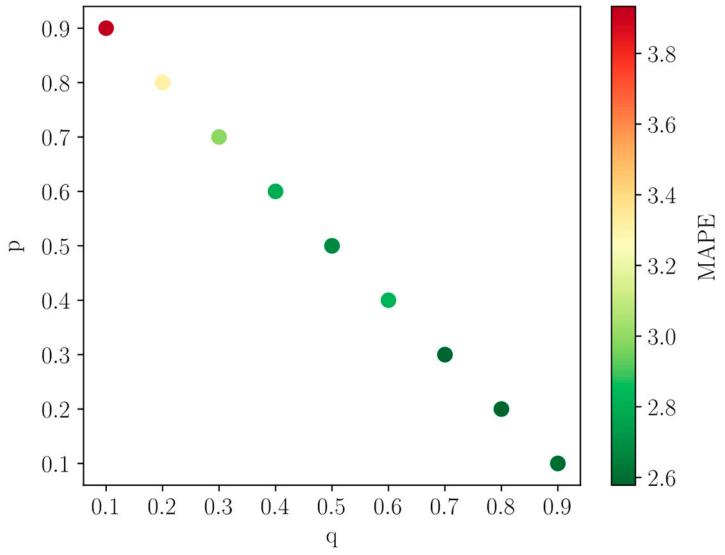

Figure 14. MAPE of different weighting factors p and q.

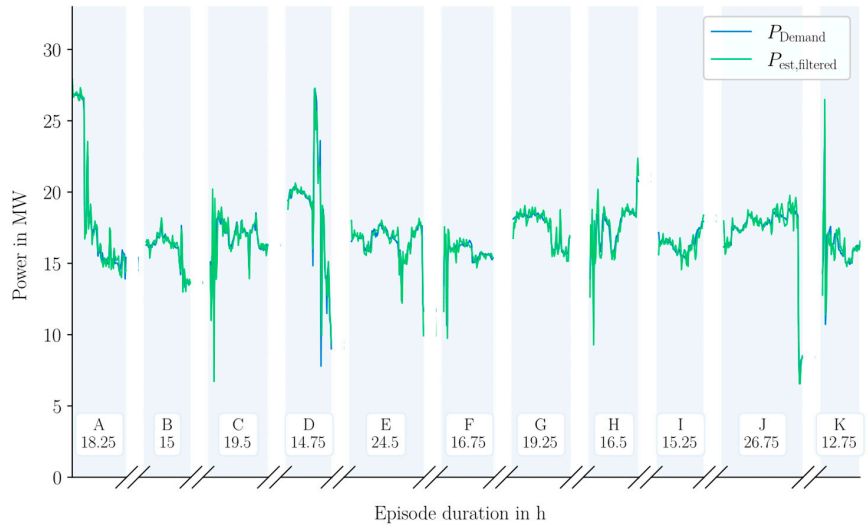

(a)

Figure 15. *Cont.*

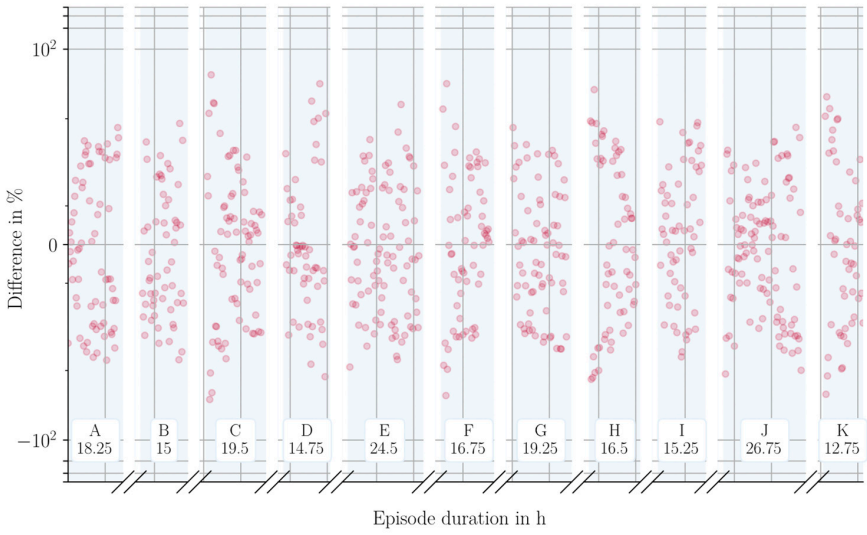

(**b**)

Figure 15. Improved estimator and error analysis using p = 0.3 and q = 0.7 with (**a**) the load curves; (**b**) the deviation of the filtered and estimated values $P_{\text{est,filtered}}$ from the measured values P_{Demand} in percent shown on a logarithmic scale as red points.

4.2. Look-Ahead Energy Management Method

Building on the filtered estimator of the load demand, a new EMS strategy that predicts the load distribution is defined. In doing so, it is assumed that the ship, as described in the previous chapter, travels on planned routes at reasonably predictable speeds over ground. Under these assumptions, it can be assumed that the required speed and position of the ship for a future period at any point in time are known. With the aid of the estimator developed in the previous section, the load demand for future time events can be predicted and the load distribution can be adjusted appropriately.

4.2.1. Definition of the Energy Management Method

Starting at a time t, the future load β_{LA}·15 min is predicted, with β_{LA} as a configurable look-ahead factor of the energy management method to determine the forecast time horizon. The filtered estimator $\hat{P}_{\text{est.,filtered}}$ to predict the power demand of the ship is used. We want to average these predicted load values to an arithmetic mean $\overline{P}_{LA}(t)$. $\overline{P}_{LA}(t)$ thus represents the estimated mean load for the time $t = t_0 + \beta_{LA}$·15 min.

In addition, SOC(t) was utilized to denote the current state of charge of the battery and (SOC_{min},SOC_{max}) to define an interval that the SOC should not leave if the load scenario allows. In the following, interval limits of (SOC_{min},SOC_{max}) = (40%,70%) will be used to maintain a safe operational window of the battery. At first, a dynamic range for the output power of the SOFC is defined with

$$\mathrm{P}_{\text{SOFC,min}}(t) := \overline{P}_{LA}(t) + \frac{1}{\Delta t}(SOC_{min} - SOC(t))\cdot C_{Bat}, \tag{14}$$

and

$$\mathrm{P}_{\text{SOFC,max}}(t) := \overline{P}_{LA}(t) + \frac{1}{\Delta t}(SOC_{max} - SOC(t))\cdot C_{Bat}, \tag{15}$$

which the SOFC should not leave. Based on this, the power $P_{\text{SOFC,demand}}$ requested by the energy management from the SOFC at time t is set as follows:

$$P_{\text{SOFC,demand}}(t) := \begin{cases} P_{\text{SOFC,min}}(t), \; if \; P_{\text{SOFC,demand}}(t) < P_{SOFC}(t) \\ P_{\text{SOFC,max}}(t), \; if \; P_{\text{SOFC,demand}}(t) > P_{SOFC}(t), \\ P_{SOFC}(t), \; else \end{cases} \tag{16}$$

With these rules, an EMS with the following two goals is developed:

1. The SOC should be kept over time in a pre-definable operational range to keep the battery in a safe operational window and avoid degradation due to a higher depth of discharge [41].
2. The SOFC should change its output power only if it is foreseeable that a deviating average power is to be provided by the propulsion system.

Figure 16 shows the functionality of the EMS.

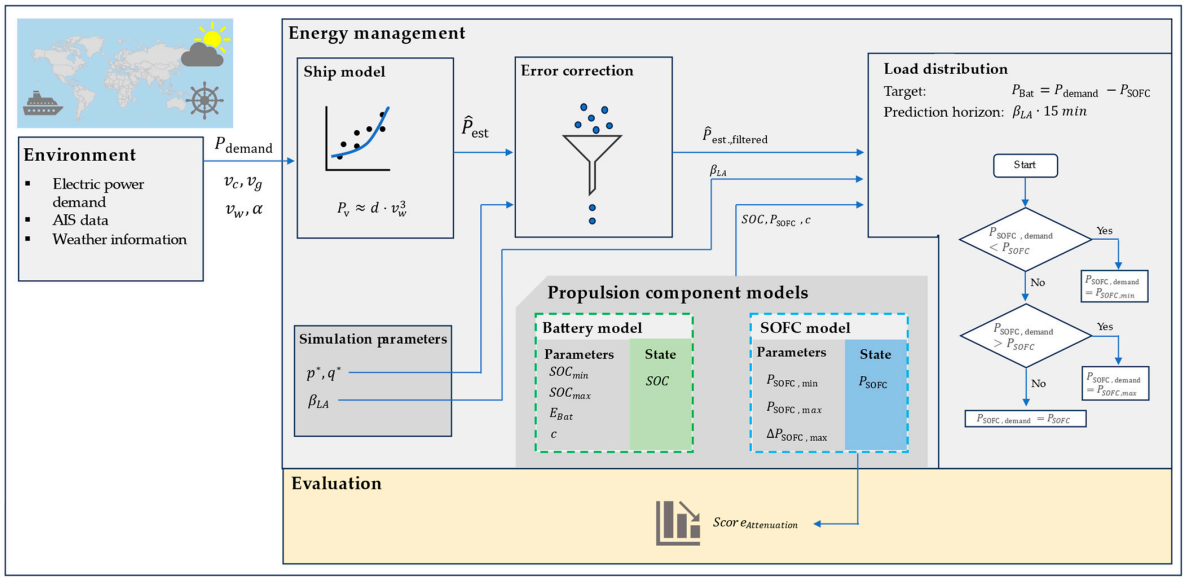

Figure 16. Schematic overview of the functionality of the look-ahead energy management method.

4.2.2. Simulation of the EMS and Performance Check

In Figure 17, the power distribution of the look-ahead EMS is shown. Compared to the power split of the rule-based energy management method shown in Figure 9, the SOFC no longer strictly tries to follow the load demand of the system. We can even see periods in individual episodes where the actual output power of the SOFC remains constant. In return, the battery must compensate for more power differences in the load demand.

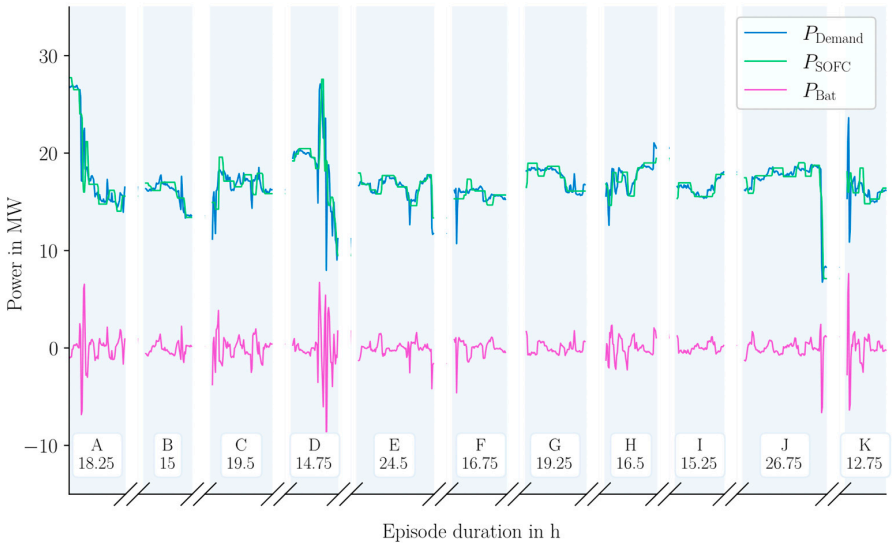

Figure 17. Resulting power split of the look-ahead strategy simulation with $\beta_{LA} = 4$ and SOC_{min}, SOC_{max} = (40%, 70%).

The attenuation score for the SOFC is shown in Figure 18 for the look-ahead strategy. Table 5 shows the resulting attenuation score values for both methods. It shows that the score of the look-ahead strategy is lower for all episodes, which is an indication of less transient events and an overall steadier operation of the SOFC system. Figure 19 shows a detailed view of episode A.

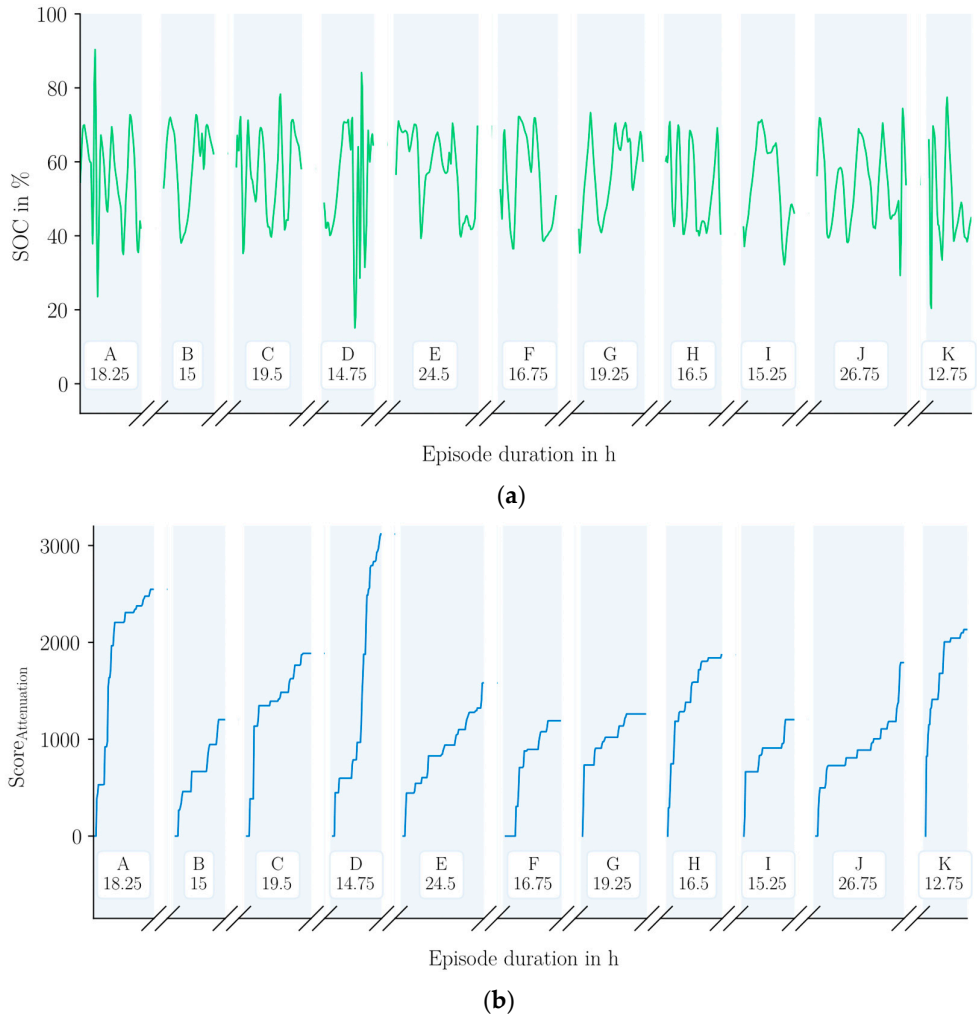

Figure 18. (**a**) *SOC*; (**b**) attenuation score of the SOFC for the look-ahead strategy with $\beta_{LA} = 4$ and SOC_{min}, SOC_{max} = (40%, 70%).

Table 5. Aging score of the SOFC for the proposed look-ahead strategy and the rule-based EMS.

Episode	$Score_{Attenuation}$	
	Look-Ahead	**Rule-Based EMS**
A	2546	3113
B	1202	2206
C	1886	3028
D	3119	4529
E	1582	2173
F	1191	2336
G	1261	1692
H	1872	2793
I	1202	1626
J	1791	2036
K	2132	3579

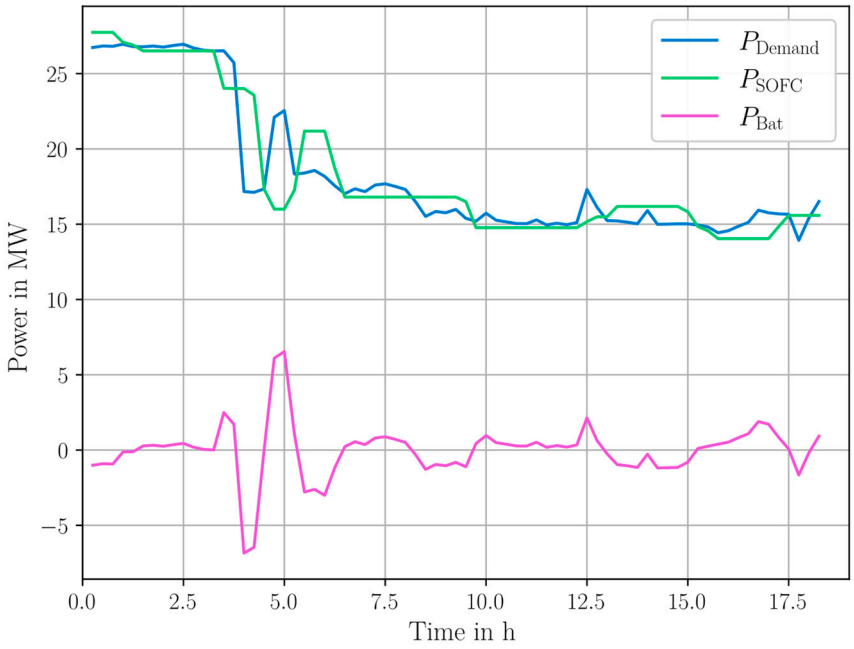

Figure 19. Detailed view of the power split of episode A for the look-ahead strategy.

The results indicate the effectiveness of the suggested look-ahead EMS strategy, which should lead to a reduction of stress factors on the SOFC caused by high dynamics. Moreover, the utilization of the battery system is much higher, which could lead to higher cyclic aging of the battery. However, the battery is proportionally much smaller than the SOFC and the size ratio of the components should be in line with the savings that can be realized by prolonging its service life.

5. Discussion

This work aimed to investigate the extent to which an EMS for a hybrid ship propulsion system can benefit from the use of additional data sources. We quantitatively investigated external influences on a ship to be able to predict the future load demand. Predicting the future load demand of a ship seems to be a reasonable method to maintain a steady-state operation for power sources with low dynamic capabilities. The rigid route planning in shipping, which makes reliable forecasting over longer periods possible in the first place, is particularly helpful here. Unlike in automobile traffic, ships rarely have to react to spontaneous events on long sections of the route, so that a planned route can usually be executed. Most of the environmental influences acting on the ship can be suitably modeled and predicted to a certain extent considering the hydrodynamic properties of the investigated vessel so that an EMS strategy that adjusts its behavior based on predictions of future load demand seems to be a reasonable method which can be realized without high computational burden.

After modeling the physical relationships and selecting appropriate data sets to determine the model parameters, an estimator for the load demand of a cruise ship was developed, and the accuracy of the prediction was compared against real measurement data. This yielded an accuracy of 7.68%, which would still represent powers in the multi-MW-range for such a large application. Since the upper limits of the battery power capability could be exceeded in this case, this could present a technical issue for the hybrid drive system. The error could be decreased to 2.68% by analyzing and correcting the systemic error. This is an acceptable prediction given that the average deviation in this case is approximately 1.25 MW for the maximum power output of the investigated ship application. This load can be supplied by the battery assumed in the investigated configuration. From this, an EMS has been developed that utilizes load prediction to improve the dynamic operation of the SOFC. As the SOFC is the main propulsion component, good dynamic behavior,

which reduces the stress factors on the component, is essential for the efficient operation of the ship's propulsion system. The functionality of the EMS was verified with the help of simulations over different authentic cruise profiles.

The data-based energy management method that has been developed predicts load curves with a high degree of accuracy based on tracking and weather data and can therefore process very large amounts of data to implement a resource-efficient power distribution between the drive components. Predictions are realized without the implementation of neuronal networks or regression models which can be resource-intensive to set up, train, and tune. This algorithm is therefore able to run on conventional ship control systems and is therefore a retrofit option. In addition, the use of this EMS is relevant for an economic operation, as the procurement and commissioning of SOFCs has comparatively high costs [42]. By reducing stress factors, a longer service life of the SOFC can be achieved, which could significantly reduce the operating costs of this ship application.

However, despite the interesting results, the explanations of this work have a few shortcomings, which could be overcome in future work. For example, due to a lack of data, the simulation could only be performed for a few periods. For a more comprehensive validation, it would be interesting to study the functionality over a longer period. This could reveal further potential for improvement. Also, a higher sampling rate of the load profiles underlying the calculations and simulations would have been helpful to investigate the dynamic performance of the hybrid propulsion system in a higher level of detail.

Outlook and Future Work

The estimation function presented for the load demand does not yet represent all environmental influences. Particularly wind and waves, which have a significant influence on the power demand of a ship, could not be considered. By additional physical modeling of these effects and the use of further data, the estimation of the future load consumption of a ship could be further improved.

Besides a mapping of further environmental influences, it could also be investigated whether the estimation procedures in general can be improved. In this work, a balancing calculation was performed using polynomial function approaches and the least squares method. This could involve the use of other methods to establish a functional relationship between the measured values. A mapping with Gaussian processes or the training of suitable neural networks could improve the results in the case of large data sets.

Furthermore, the functionality of the algorithms could be validated in a hardware-in-the-loop test bench environment. Such a measurement series would allow for a precise examination of the propulsion components concerning their dynamic behavior or technical suitability for the designated application. In addition, the real-time capability of the algorithms on controllers could be verified within the test bench.

Author Contributions: Conceptualization, C.Ü. and U.H.M.; methodology, C.Ü. and U.H.M.; software, C.Ü. and U.H.M.; validation, C.Ü., U.H.M., K.L.Q. and M.F.B.; formal analysis, C.Ü., U.H.M., K.L.Q. and M.F.B.; investigation, C.Ü. and U.H.M.; resources, D.U.S.; data curation, C.Ü., A.B., F.R. and D.U.S.; writing—original draft preparation, C.Ü.; writing—review and editing, C.Ü., K.L.Q., and M.F.B.; visualization, C.Ü. and U.H.M.; supervision, C.Ü.; project administration, C.Ü., A.B., F.R. and D.U.S.; funding acquisition, C.Ü., A.B., F.R. and D.U.S. All authors have read and agreed to the published version of the manuscript.

Funding: This research was funded by the European Commission within the European Union's Horizon 2020 research and innovation program under the project NAUTILUS, grant number 861647.

Data Availability Statement: Data are contained within the article.

Conflicts of Interest: The authors declare no conflict of interest.

Nomenclature

Abbreviations	
AIS	Automatic Identification System
ECM	Equivalent circuit model
EMS	Energy management system
GPS	Global Positioning System
ICE	Internal combustion engine
LIB	Lithium-ion battery
SOC	State of charge
SOFC	Solid oxide fuel cell
Parameters	
α	Angle of the velocity vector
β_{LA}	Configurable factor to determine the prediction horizon
$c(t)$	Charge or discharge factor of the battery
C_{Bat}	Battery capacity
d	Cubic coefficient for the calculation of the relation between measured power demand and speed of the vessel
E_{Bat}	Capacity or maximum energy content of the battery
m	Mass of the vessel
η	Coulomb efficiency
η_{eff}	Drive train efficiency
$\hat{P}_{\text{Baseload,15min}}(t)$	Arithmetic mean of load demand in harbor mode for 15 min time resolution
$P_{\text{Bat}}(t)$	Power provided or drawn by the battery at time t
$P_{\text{Bat,max}}$	Maximum power out-/input of the battery
P_{charge}	Absolute in- or output power of the battery
$P_{\text{est}} = \hat{P}(t, v_g, \Delta v_g, v_w)$	Mean estimated power demand for given velocities
$\hat{P}_{\text{est.,filtered}}(t)$	Filtered estimated power demand
$\Delta\hat{P}_{kin,15min}(t)$	Change in power after a time step required for propulsion
$P_{\text{SOFC}}(t)$	Actual power provided by the fuel cell at time t
$P_{\text{SOFC,demand}}(t)$	Power demand applied to the fuel cell at time t
$P_{\text{SOFC,min}}$	The minimum power output of the fuel cell; 0 W in the presented simulation
$\Delta P_{\text{SOFC,max}}$	Rate of change of the output power of the solid oxide fuel cell
$P_{\text{SOFC,max}}$	The maximum power output of the fuel cell
SOC_{min}	Lower SOC boundary for the simulation
SOC_{max}	Upper SOC boundary for the simulation
U_{Cell}	Battery cell voltage
U_{OCV}	Battery cell open circuit voltage
v_c, $\vec{v}_c(t)$	Velocity of ocean currents
v_g, $\vec{v}_g(t)$	Velocity over ground
v_w, $\vec{v}_w(t)$	Velocity through water

References

1. United Nations Conference on Trade and Development. *50 Years of Review of Maritime Transport, 1968–2018: Reflecting on the Past, Exploring the Future*; No. UNCTAD/DTL/2018/1; United Nations Conference on Trade and Development: Geneva, Switzerland, 2018.
2. International Maritime Organization. Fourth IMO GHG Study 2020. 2021. Available online: https://wwwcdn.imo.org/localresources/en/OurWork/Environment/Documents/Fourth%2520IMO%2520GHG%2520Study%25202020%2520-%2520Full%2520report%2520and%2520annexes.pdf (accessed on 31 October 2023).
3. Mallouppas, G.; Yfantis, E.A. Decarbonization in Shipping Industry: A Review of Research, Technology Development, and Innovation Proposals. *J. Mar. Sci. Eng.* **2021**, *9*, 415. [CrossRef]
4. Chin, C.S.; Tan, Y.-J.; Kumar, M.V. Study of Hybrid Propulsion Systems for Lower Emissions and Fuel Saving on Merchant Ship during Voyage. *J. Mar. Sci. Eng.* **2022**, *10*, 393. [CrossRef]
5. Kolodziejski, M.; Michalska-Pozoga, I. Battery Energy Storage Systems in Ships' Hybrid/Electric Propulsion Systems. *Energies* **2023**, *16*, 1122. [CrossRef]
6. Kersey, J.; Popovich, N.D.; Phadke, A.A. Rapid battery cost declines accelerate the prospects of all-electric interregional container shipping. *Nat. Energy* **2022**, *7*, 664–674. [CrossRef]
7. Dokiya, M. SOFC system and technology. *Solid. State Ion.* **2002**, *152–153*, 383–392. [CrossRef]

8. Fang, Q.; Blum, L.; Stolten, D. Electrochemical Performance and Degradation Analysis of an SOFC Short Stack Following Operation of More than 100,000 Hours. *J. Electrochem. Soc.* **2019**, *166*, F1320–F1325. [CrossRef]
9. Machaj, K.; Kupecki, J.; Malecha, Z.; Morawski, A.W.; Skrzypkiewicz, M.; Stanclik, M.; Chorowski, M. Ammonia as a potential marine fuel: A review. *Energy Strategy Rev.* **2022**, *44*, 100926. [CrossRef]
10. Lin, Y.; Zhan, Z.; Liu, J.; Barnett, S. Direct operation of solid oxide fuel cells with methane fuel. *Solid. State Ion.* **2005**, *176*, 1827–1835. [CrossRef]
11. Fan, L.; Tu, Z.; Chan, S.H. Recent development of hydrogen and fuel cell technologies: A review. *Energy Rep.* **2021**, *7*, 8421–8446. [CrossRef]
12. Obara, S. Dynamic-characteristics analysis of an independent microgrid consisting of a SOFC triple combined cycle power generation system and large-scale photovoltaics. *Appl. Energy* **2015**, *141*, 19–31. [CrossRef]
13. Shen, M. Solid oxide fuel cell-lithium battery hybrid power generation system energy management: A review. *Int. J. Hydrogen Energy* **2021**, *46*, 32974–32994. [CrossRef]
14. Zhang, L.; Xie, H.; Niu, Q.; Wang, F.; Xie, C.; Wang, G. Optimization of energy management in hybrid SOFC-based DC microgrid considering high efficiency and operating safety when external load power goes up. *Sustain. Energy Fuels* **2023**, *7*, 1433–1446. [CrossRef]
15. Wu, Z.; Zhu, P.; Yao, J.; Tan, P.; Xu, H.; Chen, B.; Yang, F.; Zhang, Z.; Porpatham, E.; Ni, M. Dynamic modeling and operation strategy of natural gas fueled SOFC-Engine hybrid power system with hydrogen addition by metal hydride for vehicle applications. *ETransportation* **2020**, *5*, 100074. [CrossRef]
16. Wang, X.; Zhu, J.; Han, M. Industrial Development Status and Prospects of the Marine Fuel Cell: A Review. *J. Mar. Sci. Eng.* **2023**, *11*, 238. [CrossRef]
17. Valadez Huerta, G.; Álvarez Jordán, J.; Marquardt, T.; Dragon, M.; Leites, K.; Kabelac, S. Exergy analysis of the diesel pre-reforming SOFC-system with anode off-gas recycling in the SchIBZ project. Part II: System exergetic evaluation. *Int. J. Hydrogen Energy* **2019**, *44*, 10916–10924. [CrossRef]
18. van Veldhuizen, B.N.; van Biert, L.; Amladi, A.; Woudstra, T.; Visser, K.; Aravind, P.V. The effects of fuel type and cathode off-gas recirculation on combined heat and power generation of marine SOFC systems. *Energy Convers. Manag.* **2023**, *276*, 116498. [CrossRef]
19. Kistner, L.; Schubert, F.L.; Minke, C.; Bensmann, A.; Hanke-Rauschenbach, R. Techno-economic and Environmental Comparison of Internal Combustion Engines and Solid Oxide Fuel Cells for Ship Applications. *J. Power Sources* **2021**, *508*, 230328. [CrossRef]
20. van Biert, L.; Godjevac, M.; Visser, K.; Aravind, P.V. A review of fuel cell systems for maritime applications. *J. Power Sources* **2016**, *327*, 345–364. [CrossRef]
21. Dinu, O.; Ilie, A.M. Maritime vessel obsolescence, life cycle cost and design service life. *IOP Conf. Ser. Mater. Sci. Eng.* **2015**, *95*, 12067. [CrossRef]
22. Khan, M.Z.; Mehran, M.T.; Song, R.-H.; Lee, S.-B.; Lim, T.-H. Effects of applied current density and thermal cycling on the degradation of a solid oxide fuel cell cathode. *Int. J. Hydrogen Energy* **2018**, *43*, 12346–12357. [CrossRef]
23. Hanasaki, M.; Uryu, C.; Daio, T.; Kawabata, T.; Tachikawa, Y.; Lyth, S.M.; Shiratori, Y.; Taniguchi, S.; Sasaki, K. SOFC Durability against Standby and Shutdown Cycling. *J. Electrochem. Soc.* **2014**, *161*, F850–F860. [CrossRef]
24. Ma, Z.; Chen, H.; Han, J.; Chen, Y.; Kuang, J.; Charpentier, J.-F.; Aït-Ahmed, N.; Benbouzid, M. Optimal SOC Control and Rule-Based Energy Management Strategy for Fuel-Cell-Based Hybrid Vessel including Batteries and Supercapacitors. *J. MAR. SCI. ENG.* **2023**, *11*, 398. [CrossRef]
25. Dinh, T.Q.; Bui, T.M.; Marco, J.; Watts, C.; Yoon, J.I. Optimal Energy Management for Hybrid Electric Dynamic Positioning Vessels. *IFAC-Pap.* **2018**, *51*, 98–103. [CrossRef]
26. Bui, T.M.N.; Dinh, T.Q.; Marco, J.; Watts, C. Development and Real-Time Performance Evaluation of Energy Management Strategy for a Dynamic Positioning Hybrid Electric Marine Vessel. *Electronics* **2021**, *10*, 1280. [CrossRef]
27. Bassam, A.M.; Phillips, A.B.; Turnock, S.R.; Wilson, P.A. Development of a multi-scheme energy management strategy for a hybrid fuel cell driven passenger ship. *Int. J. Hydrogen Energy* **2017**, *42*, 623–635. [CrossRef]
28. Kistner, L.; Bensmann, A.; Hanke-Rauschenbach, R. Optimal Design of Power Gradient Limited Solid Oxide Fuel Cell Systems with Hybrid Storage Support for Ship Applications. *Energy Convers. Manag.* **2021**, *243*, 114396. [CrossRef]
29. Li, J.; Herdem, M.S.; Nathwani, J.; Wen, J.Z. Methods and applications for Artificial Intelligence, Big Data, Internet of Things, and Blockchain in smart energy management. *Energy AI* **2023**, *11*, 100208. [CrossRef]
30. Haseltalab, A.; Negenborn, R.R. Model predictive maneuvering control and energy management for all-electric autonomous ships. *Appl. Energy* **2019**, *251*, 113308. [CrossRef]
31. International Maritime Organization. *Resolution A. 1106(29) Revised Guidelines for the Onboard Operational Use of Shipborne Automatic Identification Systems (AIS)*; IMO: London, UK, 2015.
32. Lee, E.; Mokashi, A.J.; Moon, S.Y.; Kim, G. The Maturity of Automatic Identification Systems (AIS) and Its Implications for Innovation. *J. Mar. Sci. Eng.* **2019**, *7*, 287. [CrossRef]
33. Kim, S.-H.; Roh, M.-I.; Oh, M.-J.; Park, S.-W.; Kim, I.-I. Estimation of ship operational efficiency from AIS data using big data technology. *Int. J. Nav. Archit. Ocean. Eng.* **2020**, *12*, 440–454. [CrossRef]
34. Hoerner, S.F. *Fluid-Dynamic Drag*; Midland Park, NJ, USA, 1965. Available online: https://ia600707.us.archive.org/13/items/FluidDynamicDragHoerner1965/Fluid-dynamic_drag__Hoerner__1965_text.pdf.

35. Sündermann, J.; Pohlmann, T. A brief analysis of North Sea physics. *Oceanologia* **2011**, *53*, 663–689. [CrossRef]
36. Tadros, M.; Ventura, M.; Guedes Soares, C. Design of Propeller Series Optimizing Fuel Consumption and Propeller Efficiency. *J. Mar. Sci. Eng.* **2021**, *9*, 1226. [CrossRef]
37. Ghimire, P.; Park, D.; Zadeh, M.K.; Thorstensen, J.; Pedersen, E. Shipboard Electric Power Conversion: System Architecture, Applications, Control, and Challenges [Technology Leaders]. *IEEE Electrific. Mag.* **2019**, *7*, 6–20. [CrossRef]
38. Sakile, R.; Sinha, U.K. Estimation of lithium-ion battery state of charge for electric vehicles using a nonlinear state observer. *Energy Storage* **2022**, *4*, e290. [CrossRef]
39. Institute for Power Electronics and Electrical Drives. ISEA Framework. Available online: https://git.rwth-aachen.de/isea/framework (accessed on 26 July 2023).
40. Waag, W.; Käbitz, S.; Sauer, D.U. Experimental investigation of the lithium-ion battery impedance characteristic at various conditions and aging states and its influence on the application. *Appl. Energy* **2013**, *102*, 885–897. [CrossRef]
41. Ecker, M.; Nieto, N.; Käbitz, S.; Schmalstieg, J.; Blanke, H.; Warnecke, A.; Sauer, D.U. Calendar and cycle life study of Li(NiMnCo)O2-based 18650 lithium-ion batteries. *J. Power Sources* **2014**, *248*, 839–851. [CrossRef]
42. Whiston, M.M.; Azevedo, I.M.; Litster, S.; Samaras, C.; Whitefoot, K.S.; Whitacre, J.F. Meeting U.S. Solid Oxide Fuel Cell Targets. *Joule* **2019**, *3*, 2060–2065. [CrossRef]